Low temperature synthesis of bioactive materials

(Síntese de materiais bioativos a baixas temperaturas)

L. C. Bandeira[1], P. S. Calefi[1], K. J. Ciuffi[1], E. J. Nassar[1], I. M. M. Salvado[2], M. H. F. V. Fernandes[2]
[1]Universidade de Franca, Av. Dr. Armando Salles Oliveira 201, Pq. Universitário, Franca, SP, Brazil 14404-600
[2]Departamento de Engenharia Cerâmica e do Vidro, Universidade de Aveiro - CICECO, 3810, Aveiro, Portugal
ejnassar@unifran.br

Abstract

Bioactive materials possess properties that allow them to interact with natural tissues to induce reactions that favor the development and regeneration of those tissues. In this study, silica was prepared by the sol-gel method, using tetraethylorthosilicate as the precursor. The calcium and phosphor sources used here were calcium ethoxy and phosphoric acid, respectively, in ethanol solvent. The solid obtained was dried at 50 °C. In vitro bioactivity assays were performed by soaking the materials in simulated body fluid (SBF). The samples were characterized by transmission electron microscopy (TEM), thermal analysis and photoluminescence. TEM images of the samples before contact with SBF revealed amorphous aggregates and after 12 days in SBF showed two phases, one amorphous with large quantities of Si and O, and the other a crystalline phase whose composition contained Ca and P. The electron diffraction pattern showed a planar distance of 2.86 Å, corresponding to 2θ = 32.2°. This was ascribed to hydroxyapatite. The Eu III was used as structural probe. The relative band intensity correspondent the transition $^5D_0 \rightarrow {}^7F_2$ / $^5D_0 \rightarrow {}^7F_1$ showed a high symmetry surrounding the Eu III ion. These materials, produced by the sol-gel route, open up new possibilities for obtaining bioactive biomaterials for medical applications.
Keywords: biomaterials, europium III, sol-gel, nanoparticles, hydroxyapatite.

Resumo

Os materiais bioativos apresentam propriedades que permitem a sua interação com um tecido de origem natural podendo induzir a sua regeneração. Neste estudo, o método sol-gel foi utilizado para a preparação de sílica dopada com íons cálcio e fósforo, partindo dos precursores tetraetilortosilicato, etóxido de cálcio e ácido fosfórico em etanol como solvente. O sólido obtido foi seco a 50 ºC. Ensaios de bioatividade foram realizados in vitro em uma solução que simula o fluido corpóreo (SBF). As amostras foram caracterizadas por microscopia eletrônica de transmissão (MET), análise térmica e fotoluminescência. As imagens de MET das amostras antes do contato com SBF revelou a presença de aglomerados amorfos. Depois de 12 dias em SBF a amostra apresentou duas fases, uma amorfa com grande quantidade de silício e oxigênio, e outra cristalina contendo cálcio e fósforo. A difração de elétrons mostrou uma distância planar de 2,86 Å, correspondendo a 2θ = 32,2°. Esse ângulo foi atribuído ao principal pico da hidroxiapatita. O íon Eu III foi usado como sonda estrutural, apresentando em seu espectro de emissão uma intensidade relativa entre as transições $^5D_0 \rightarrow {}^7F_2$ / $^5D_0 \rightarrow {}^7F_1$ que indica um ambiente de alta simetria para este íon. Estes materiais obtidos pelo método sol-gel a baixa temperatura apresentam possibilidade de se obter biomateriais bioativos para aplicação em medicina.
***Palavras-chave**: biomateriais, európio III, sol-gel, nanopartículas, hidróxiapatita.*

INTRODUCTION

Every year, thousands of patients around the world require bone implants due to aging, bone defects arising from trauma, tumors, bone diseases and other causes. Several constraints, such as availability, storage, and others, have hindered implantation with natural bone [1].

Tissue engineering has been defined as the application of scientific principles to the design, construction, modification and growth of living tissues using biomaterials, cells and factors, alone or in combination [2]. Hydroxyapatite (HA) is widely used as a bone substitute to fill bone defects or to coat prosthetic metal in order to promote its biocompatibility. However, analyses of tissues retrieved from unsuccessful implants have suggested that phagocytosis of HA wear debris by monocytes/macrophages may provide a potent stimulus for the release of a variety of cytokines [3]. In 1971, a new biomaterial was introduced – Bioglass® 45S5 – which showed the ability to bond to bone through the formation of a HA surface layer [4]. In the last few years, materials with high levels of bioactivity have increased the formation of HA layers, because of the mechanically strong bond that bioactive implants form with bone [5-8].

In the future, biomaterials are expected to enhance the regeneration of natural tissues, promoting the restoration of structure, function, metabolic and biochemical behavior, and biomechanical performance [7].

The new materials have been employed in a variety of implant applications, as indicated in a comprehensive review on the subject published recently by Liu and Webster [9]. In

addition, several research works have discussed a variety of materials used in bone implantation. One of these materials is silicon, a substrate commonly used in microimplants but which can produce undesirable interactions with the human immune system, thus requiring the use of biomolecules [10]. Another study synthesized and evaluated a novel polyurethane-based injectable *in situ* curable polymer platform to determine its potential uses as a tissue-engineered implant [11]. Carbon nanotubes have also been studied by possible applications in implants, thanks to their excellent mechanical properties as reinforcements, imparting strength and toughness to brittle hydroxyapatite bioceramic coating [12]. In addition, protein can be used as a tissue-engineering strategy for bone regeneration [13]. Glass and ceramics containing $CaO\text{-}P_2O_5\text{-}SiO_2$, *in vivo*, have shown properties such as osteoconductivity and osteoinductivity [14-16].

Hydroxyapatite and calcium carbonate are biominerals that can be combined with glasses and/or organic polymers to form biocompatible hybrid, organic-inorganic materials [1, 17-20]. Moreover, sol-gel processes are now used to produce bioactive coatings, powders and substrates that offer molecular control over the incorporation and biological behavior of proteins, and cells with applications as implants and sensors [5, 21, 22].

Natural bone is an inorganic-organic composite consisting mainly of nanohydroxyapatite and collagen fibers. Hybrid materials obtained by the sol-gel route combine the advantages of both organic and inorganic properties. Several kinds of precursors of organofunctional alkoxysilanes have been studied in the preparation of silica nanoparticles. The sol-gel process is based on the hydrolysis and condensation of metal or silicon alkoxides and is used to obtain a variety of high purity inorganic oxides that are simple to prepare [23, 24]. This process can be employed to obtain and prepare functionalized silica with controlled particle size and shape [25-30].

Hybrid inorganic-organic nanocomposites first appeared about 20 years ago, and the sol-gel process was the main technique whose conditions proved suitable to produce these materials and provide nanoscale combinations of inorganic and organic composites [31]. The sol-gel process presents advantages to obtain homogeneous hybrid materials under low temperature, allowing for the incorporation of a variety of compounds [32-37].

In this work, materials containing Ca-P-Si were prepared by mixing tetraethylorthosilicate (TEOS), calcium alkoxide and phosphoric acid synthesized by the sol-gel route. The matrix was prepared by the hydrolysis and condensation of the alkoxide, using basic catalysis. Europium chloride was used as a structural probe due to its luminescence properties and the possibility of its exchange with calcium ion in the phosphate, allowing for the study of the chemical surroundings. The resulting xerogel structure were analyzed before and after contact with SBF by thermal analysis (TG/DTA/DSC), photoluminescence (PL), transmission electron microscopy (TEM) and energy dispersive X-ray spectroscopy (EDX).

EXPERIMENTAL

The material was synthesized by the sol-gel route. In 10 mL of ethanol (solvent) were added $9.60x10^{-3}$ mol of TEOS, $3.84x10^{-3}$ mol of calcium ethoxide and $6.73x10^{-4}$ mol of phosphoric acid, under stirring, basic catalysis (NH_3 ethanolic saturated solution) was used. Europium III chloride in ethanolic solution was added as structural probe. After 5 h gel was formed, the bulk was obtained after dried at 50 °C during 1 day.

The sample was characterized by thermal analysis (TG/DTG), photoluminescence (PL), transmission electron microscopy (TEM) and energy-dispersive X-ray spectroscopy (EDX), then immersed in Simulated Body Fluid (SBF) [38], pH = 7.40 during 12 days. The sample was characterized before and after contat with SBF. The thermal analysis was carried out in a thermal analyzer (TA Instruments SDT Q600, Simultaneous DTA-TG) in a nitrogen atmosphere, at a heating rate of 20 °C.min^{-1} from 25 to 1500 °C. The luminescence data was obtained with a Spex Fluorolog II spectrofluorometer at room temperature. The emission was collected at 22.5° (front face) from the excitation beam. The morphology of the system was investigated by TEM, analyzing a droplet of the suspension deposited on a copper grid. The TEM analysis was performed with a 200 kV Philips CM 200 microscope.

RESULTS AND DISCUSSION

Figs. 1 and 2 show the thermogravimetric curve and derivate of the matrix Ca-P-Si dried at 50 °C before and after contact with SBF, respectively.

The matrix displayed different behaviors before and after contact with the SBF solution. Before contact, the matrix showed a 45% weight loss. The first stage, which appeared at 100 °C, was ascribed to water and solvent molecules adsorbed

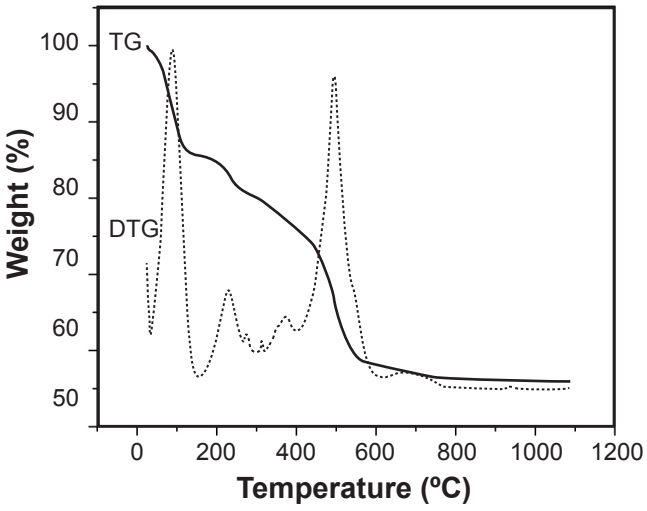

Figure 1: TG and DTG curves of the matrix Ca-P-Si before contact with SBF.

[Figura 1: Curvas TG e DTG da matriz de Ca-P-Si antes do contato com SBF.]

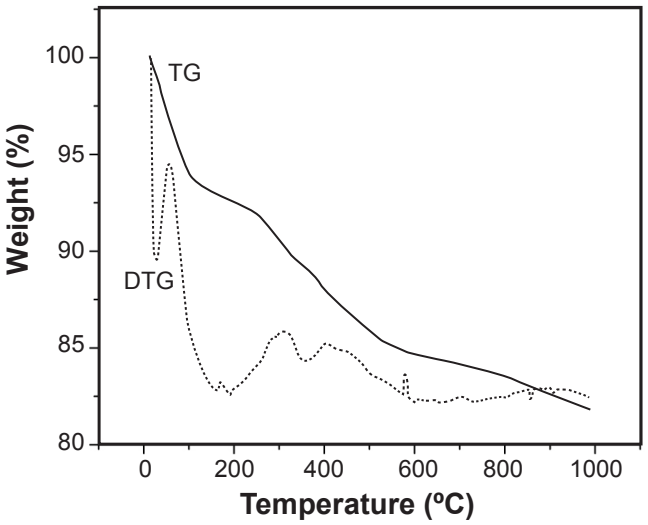

Figure 2: TG and DTG curves of the matrix Ca-P-Si after contact with SBF.
[Figura 2: Curvas TG e DTG da matriz de Ca-P-Si depois do contato com SBF.]

in the matrix, while the other stages, which took place between 200 and 650 ºC, were possibly due to the decomposition of residual organic groups of the precursor. After contact with the SBF, the matrix showed a weight loss of only 17%, which was ascribed to the migration of residual organic groups into the solution and to the deposition at surface of a mineral phase constituted by calcium phosphate. This deposition mineral phase is to thin to be responsible for such a drop of weight loss, as confirmed by transmission electron microscopy.

Fig. 3 shows the excitation spectra of the Ca-P-Si matrix doped with Eu III ions by the sol-gel method. The maximum emission was found to occur at 612 nm ($^5D_0 \rightarrow {}^7F_2$). Note the band from $^7F_0$ (fundamental level) to $^5L_6$ (excitation level) and the wide band at 250 nm, which was ascribed to the charge transfer band (CTB). The spectra's intensities were normalized.

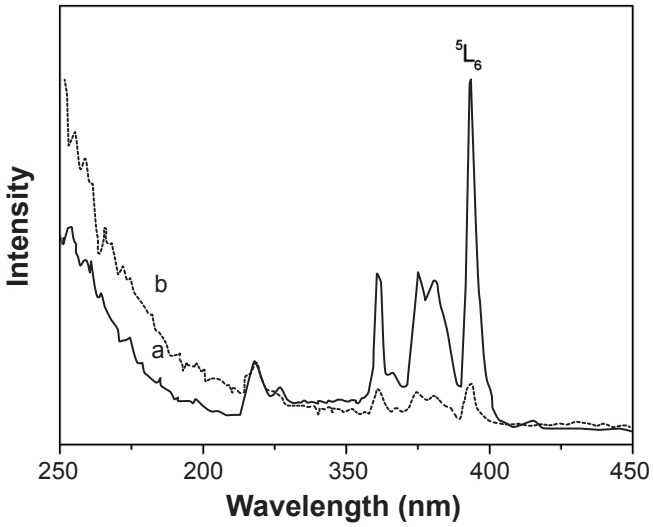

Figure 3: Excitation spectra of the Ca-P-Si matrix doped with Eu III ions before (a) and after (b) contact with SBF, $\lambda_{em.} = 612$ nm.
[Figura 3: Espectros de excitação do íon Eu III dopado na matriz de Ca-P-Si antes (a) e depois (b) contato com SBF, $\lambda_{em.} = 612$ nm.]

Fig. 4 depicts the emission spectra of the Ca-P-Si matrix doped with Eu III ions, showing the excitation wavelength in $^5L_6$ level (394 nm).

The emission spectra presented transitions arising from $^5D_0$ to ^7F_J (J = 0, 1, 2, 3 and 4) manifolds. The Eu III emission bands in these spectra are characterized by nonhomogenous distributions of the ion in the Ca-P-Si matrix [39- 41]. The band corresponding to $^5D_0 \rightarrow {}^7F_0$ transitions at 579 nm is due to sites without inversion centers occupied by Eu III ions.

Because of its electrical-dipolar nature, [42] the relative intensity of the $^5D_0 \rightarrow {}^7F_0$ and $^5D_0 \rightarrow {}^7F_2$ transitions was strongly dependent on the surrounding Eu III. The corresponding band of $^5D_0 \rightarrow {}^7F_1$ transitions had a magnetic-

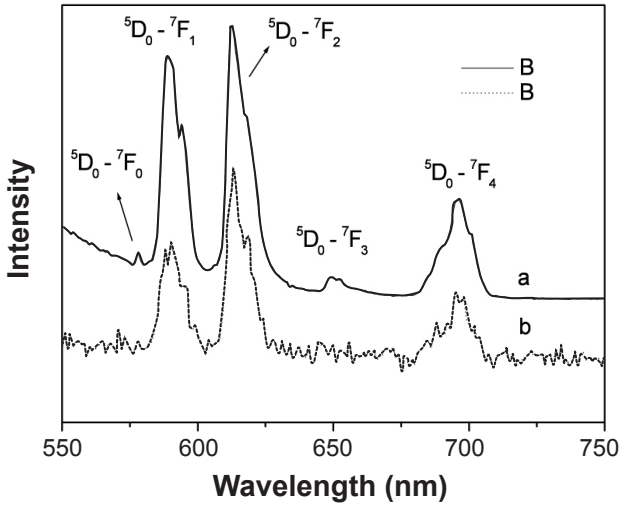

Figure 4: Emission spectra of the Ca-P-Si matrix doped with Eu III ions before (a) and after (b) contact with SBF, $\lambda_{exc.} = 394$ nm.
[Figura 4: Espectros de emissão do íon Eu III dopado na matriz de Ca-P-Si antes (a) e depois (b) contato com SBF, $\lambda_{exc.} = 394$ nm.]

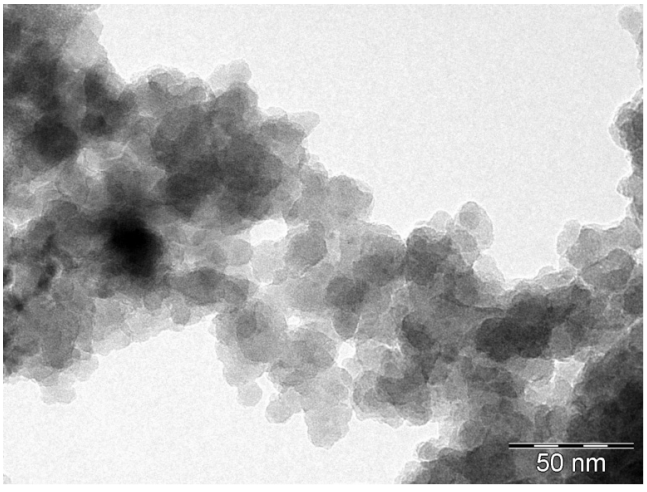

Figure 5: TEM images of the Ca-P-Si matrix before immersion in SBF.
[Figura 5: Imagens de MET da matriz de Ca-P-Si antes da imersão em SBF.]

Table I - Relative intensity ratio of $^5D_0 \rightarrow ^7F_0$ / $^5D_0 \rightarrow ^7F_1$ and $^5D_0 \rightarrow ^7F_2$ / $^5D_0 \rightarrow ^7F_1$ transitions and lifetime of the $^5D_0 \rightarrow ^7F_2$ transition.
[Tabela I - Intensidade relativa das transições $^5D_0 \rightarrow ^7F_0$ / $^5D_0 \rightarrow ^7F_1$ e $^5D_0 \rightarrow ^7F_2$ / $^5D_0 \rightarrow ^7F_1$ e o tempo de vida da transição $^5D_0 \rightarrow ^7F_2$.]

Samples	$^5D_0 \rightarrow ^7F_0$ / $^5D_0 \rightarrow ^7F_1$	$^5D_0 \rightarrow ^7F_2$ / $^5D_0 \rightarrow ^7F_1$
Before SBF	0.07	1.15
After 12 days in SBF	0.13	1.29

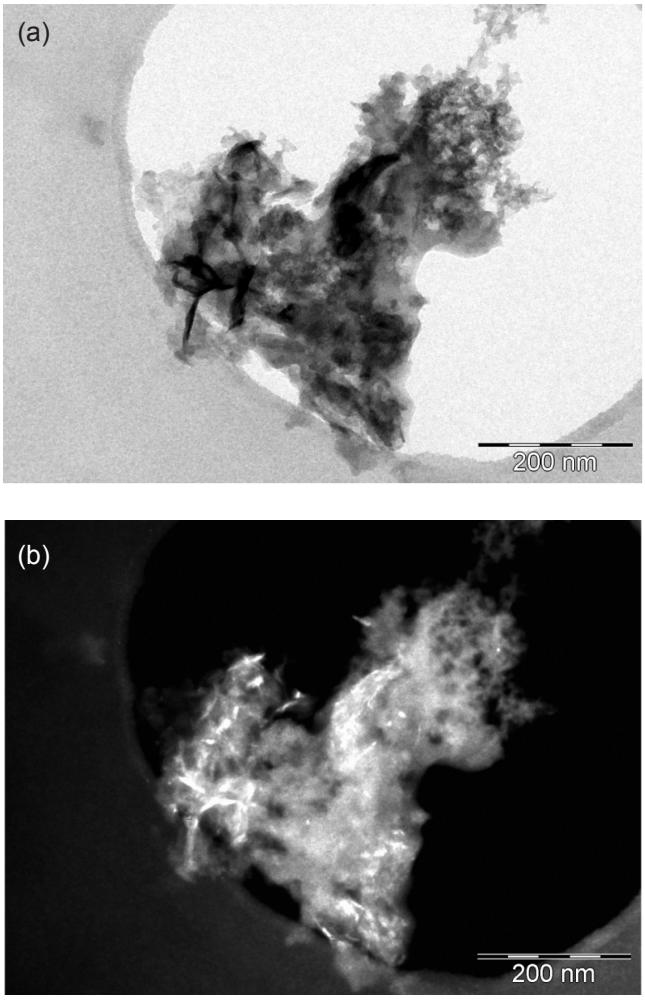

Figure 6: TEM images of the Ca-P-Si matrix after immersion in SBF; a) bright and b) dark field.
[Figura 6: Imagens de MET da matriz de Ca-P-Si depois da imersão em SBF, a) campo claro e b) campo escuro.]

dipolar nature whose intensity was unaffected by its surroundings. Therefore, it can be considered a standard to measure the relative intensity of the other bands, [43, 44] and the $^5D_0 \rightarrow ^7F_2$ emission intensity can thus provide valuable information about environmental changes around the Eu III ions. Table I shows the relative intensity of the $^5D_0 \rightarrow ^7F_0$ and $^5D_0 \rightarrow ^7F_2$ transitions in the ratio between the $^5D_0 \rightarrow ^7F_1$ transitions. The gradual increase of the ratio between transitions indicates a change in the surrounding ions.

Figure 7: Electron diffraction of the sample's crystalline phase after immersion in SBF.
[Figura 7: Difração de electrons da amostra na fase cristalina depois da imersão em SBF.]

TEM can provide structural information about materials, such as particle shape, size and crystallinity. Figs. 5 and 6 show TEM images of the Ca-P-Si matrix before and after immersion in SBF, respectively.

The TEM images in Fig. 5 reveal the formation of small particles with an average size of 20 nm. Electron diffraction revealed an amorphous phase. The bright and dark fields in Figs. 6a and b indicate that the materials have crystalline and amorphous phases. Fig. 7 shows the electron diffraction of the crystalline phase.

The electron diffraction pattern shows planar distances of 2.86 Å and 1.88 Å, which, according to Bragg's law, indicates that these distances correspond to $2\theta = 31.2$ (211) and 48.6^o (320). This peak was ascribed to hydroxyapatite (JCPDS – 9-0432) [45].

The EDX analysis served to reveal the two phases present in the materials after immersion in SBF, as indicated in Figs. 8 and 9.

The EDX spectrum of the amorphous phase reveals large quantities of Si and O, indicating amorphous silicate and lower quantities of Eu and Cl. The emission spectra of Eu III ions show a surrounding inhomogeneous site, characterizing the amorphous phase. The crystalline phase, whose composition contained Ca and P, was ascribed to the crystallization of hydroxyapatite. The matrix is an efficient biomaterial in the amorphous phase, but its level of bioactivity declines as the crystallinity increases [8].

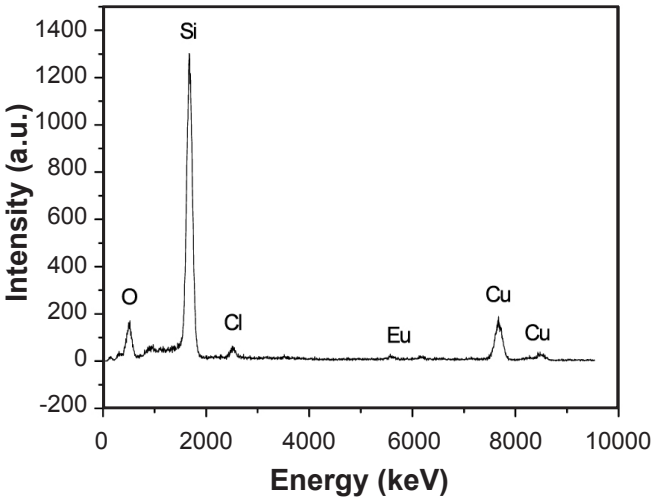

Figure 8: EDX spectrum of the sample's amorphous phase after immersion in SBF.
[Figura 8: Espectro de EDX da amostra na fase amorfo depois da imersão em SBF.]

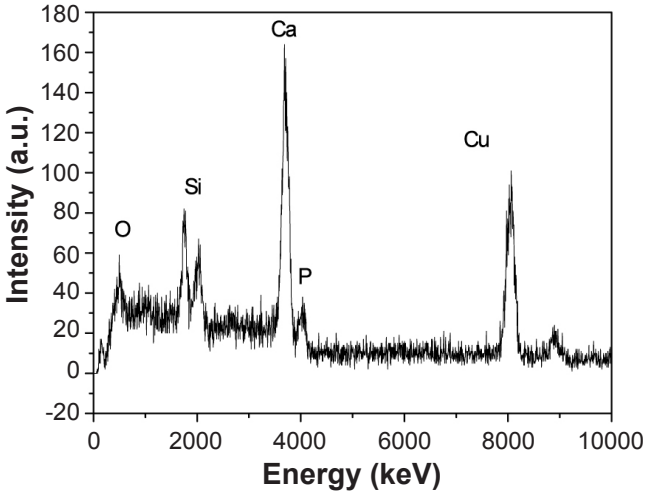

Figure 9: EDX spectrum of the sample's crystalline phase after immersion in SBF.
[Figura 9: Espectro de EDX da amostra na fase cristalina depois da imersão em SBF.]

CONCLUSION

The nanoscale combination of hybrid inorganic-organic composites offers new possibilities for obtaining new materials with special properties. Control of the nanoscale structure is the most important factor in materials for implant applications. In the case reported here, the material we developed presented good characteristics, firstly because the material was obtained on a nanoscale and secondly because the hydroxyapatite was crystalline. According to Eglin, [14] "the formation of hydroxyapatite (HA) is the first indication of a successful implant". Nevertheless, these materials still require more extensive testing. The materials produced here presented good properties for application in biomaterials. Moreover, the samples were not subjected to thermal treatment, which is a great advantage of the sol-gel method.

ACKNOWLEDGEMENTS

The authors acknowledge FAPESP, CNPq and CAPES for their financial support and are indebted to the Rare Earths Laboratory of the University of S. Paulo at Ribeirão Preto, SP, Brazil, for the luminescence data.

REFERENCES

[1] A. L. Andrade, R. Z. Domingues, *Cerâmicas Bioativas – Estado da Arte,* Química Nova **19** (2003) 100-104.
[2] F. R. A. J. Rose, R. O. C. Oreffo, *Breakthroughs and views Bone Tissue Engineering: Hope vs Hype,* Biochem. Biophys. Res. Comm. **292** (2002) 1-7.
[3] A. G. Laquerriere, O. Tabary, J. Jacquot, D. Richard, P. Frayssinet, M. Guenounou, D. L. Maquin, P. Laquerriere, S. Gangloff, *Involvement of toll-like receptor 4 in the inflammatory reaction induced by hydroxyapatite particles*, Biomater. **28** (2007) 400-404.
[4] D. C. Clupper, L. L. Hench, *Crystallization kinetics of tape cast bioactive glass 45S5*, J. Non-Crystalline Solids **318** (2003) 43-48.
[5] L. L. Hench, *Sol-gel Materials for Bioceramic Applications,* Current Opinion in Solid State & Mater. Sci. **2** (1997) 604-610.
[6] W. Cao, L. L. Hench, *Bioactive Materials,* Ceram. Int. **22** (1996) 493-507.
[7] L. L. Hench, *Biomaterials: a forecast for the future,* Biomater. **19** (1998) 1419-1423.
[8] O. Peitl, E. D. Zanotto, L. L. Hench, *Highly bioactive P_2O_5-Na_2O-CaO-SiO_2 glass-ceramics,* J. Non-Crystalline Solids **292** (2001) 115-126.
[9] H. Liu, T. H. Webster, *Nanomedicine for implants: A review of studies and necessary experimental tools,* Biomater. **28** (2007) 354-369.
[10] B. Bhushan, D. R. Tokochichu, M. T. Keener, S. C. Lu, *Morphology and adhesion of biomolecules on silicon based surfaces,* Acta Biomater. **1** (2005) 327-341.
[11] I. C. Bonzani, R. Adhikari, S. Houshyar, R. Mayadunne, P. Gunatillake, M. M. Stevens, *Synthesis of two-component injectable polyurethanes for bone tissue engineering,* Biomater. **28** (2007) 423-433.
[12] K. Balani, R. Anderson, T. Laha, M. Andara, J. Tercero, E. Crumpler, A. Agarwal, *Plasma-sprayed carbon nanotube reinforced hydroxyapatite coatings and their interaction with human osteoblasts in vitro,* Biomater. **28** (2007) 618-624.
[13] T. M. G. Chu, S. J. Warden, C. H. Turner, R. L. Stewart, *Segmental bone regeneration using a load-bearing biodegradable carrier of bone morphogenetic protein-2,* Biomater. **29** (**2**007) 459-467.
[14] D. Eglin, S. Maalheem, J. Livage, T. Coradin, *In vitro apatite forming ability of type I collagen hydrogels*

containing bioactive glass and silica sol-gel particles, J. Mater. Sci.: Materials in Medicine **17** (2000) 161-167.
[15] K. L. Skelton, J. V. Glenn, S. A. Clarke, G. Georgiou, S. P. Valappil, J. C. Knowles, S. N. Nazhat, G. R. Jordan, *Effect of ternary phosphate-based glass compositions on osteoblast and osteoblast-like proliferation, differentiation and death in vitro,* Acta Biomater. **3 (2**007) 563-572.
[16] S. K. Misra, D. Mohn, T. J. Brunner, W. J. Stark, S. E. Philip, I. Roy, V. Salih, J. C. Knowles, A. R. Boccaccini, *Comparison of nanoscale and microscale bioactive glass on the properties of P(3HB/Bioglass®) composites,* Biomater. **29 (2**008) 1750-1761.
[17] H. J. Lee, H. W. Choi, K. J. Kim, S. C. Lee, *Modification of hydroxyapatite nanosurfaces for enhanced colloidal stability and improved interfacial adhesion in nanocomposites,* Chem. Mater. **18 (2**006) 5111-5118.
[18] A. Rámila, S. Padilla, B. Muñoz, M. V. Regí, *A new hydroxyapatite/glass biphasic material: in vitro bioactivity,* Chem. Mater. **14** (2002) 2439-2443.
[19] O. Doğan, M. Öner, *Biomimetic mineralization of hydroxyapatite crystals on the copolymers of vinylphosphonic acid and 4-vinilyimodazole,* Langmuir **22** (2006) 9671-9675.
[20] T. Iwatsubo, K. Sumaru, T. Kanamori, T. Shinbo, T. Yamaguchi, *Construction of a New Artificial Biomineralization Syste,* Biomacromolecules **7 (**2006) 95-100.
[21] D. M. Pickup, R. J. Speight, J. C. Knowles, M. E. Smith, R. J. Newport, *Sol-gel synthesis and structural characterization of binary TiO_2-P_2O_5 glasses,* Mater. Res. Bull. **43** (2008) 333-342.
[22] D. Carla, D. M. Pickup, J. C. Knowles, I. Ahmed, M. E. Smith, R. J. Newport, *A structural study of sol-gel and melt-quenched phosphate-based glasses*. J. Non-Crystalline Solids **353** (2007) 1759-1765.
[23] L. A. Rocha, K. J. Ciuffi, H. C. Sacco, E. J. Nassar *Influence on deposition speed and stirring type in the obtantion of titania films.* Mater. Chem. Phys. **85 (**2004) 245-250.
[24] A. Lobnik, N. A. Majcen, K. Niederreiter, G. Uray, *Optical pH sensor based on the absorption of antenna generated europium luminescence by bromothymolblue in a sol–gel membrane,* Sensors Actuators B **74** (2001) 200-206.
[25] E. J. Nassar, K. J. Ciuffi, S. J. L. Ribeiro, Y. Messaddeq, *Europium incorporated in silica matrix obtained by sol-gel: luminescent materials,* Mater. Res. **6**, 4 (2003) 557-562.
[26] F. Beari, M. Brand, P. Jenkner, R. Lehnert, H. J. Metternich, J. Monkiewicz, H. W. Siesler, *Organofunctional alkoxysilanes in dilute aqueous solution: new accounts on the dynamic structural mutability,* J. Organo Chem. **625** (2001) 208-216.
[27] E. J. Nassar, C. R. Neri, P. S. Calefi, O. A. Serra, *Functionalized Silica synthesized by sol-gel process,* J. Non-Crystalline Solids **247** (1999) 124-128.
[28] W. Stöber, A. Fink, E. Bohn, *Controlled growth of monodisperse silica spheres in the micron size range*, J. Colloid Interface Sci. **26** (1968) 62-69.
[29] A. T. Papacídero, L. A. Rocha, B. L. Caetano, E. Molina, H. C. Sacco, E. J. Nassar, Y. Martinelli, C. Mello, S. Nakagaki, K. J. Ciuffi, *Preparation and characterization of spherical silica–porphyrin catalysts obtained by the sol–gel methodology,* Colloid Surfaces **275** (2006) 27-35.
[30] E. J. Nassar, E. C. O. Nassor, L. R. Ávila, P. F. S. Pereira, A. Cestari, L. M. Luz, K. J. Ciuffi, P. S. Calefi, *Spherical hybrid silica particles modified by methacrylate groups*, J. Sol-Gel Sci. Technol. **43 (**2007) 21-26.
[31] K. C. Vrancken, K. Possemiers, P. V. D. Voort, E. F. Vansant, *Surface modification of silica gels with aminoorganosilanes*. Colloids Surface A: Physicochem. Eng. Aspects **98** (1995) 235-241.
[32] J. E. Mark, C. Y. C. Lee, P. A. Bianconi, *Hybrid Organic-Inorganic Composites,* ACS Symp. Ser. 586, Am. Chemical Soc. Washington, DC (1995).
[33] G. Cerveau, R. J. P. Corriu, C. Lepeytre, P. H. Mutin, *Influence of the nature of the organic precursor on the textural and chemical properties of silsesquioxane materials,* J. Mater. Chem. **12 (**1998) 2707-2713.
[34] R. Corriu, *A new trend in metal-alkoxide chemistry: the elaboration of monophasic organic-inorganic hybrid materials,* Polyhedron **17** (1998) 925-934.
[35] R. J. P. Corriu, D. Leclerq, *Recent Developments of Molecular Chemistry for Sol-Gel Processes,* Angew. Chem. Int. Engl. **35** (1996**)** 1420-1436.
[36] K. J. Shea, D. A. Loy, O. Webster, *Arylsilsesquioxane gels and related materials: New hybrids of organic and inorganic networks*. J. Am. Chem. Soc. **114** (1992) 6700-6710.
[37] C. L. Jackson, B. J. Bauer, A. I. Nakatami, J. Barnes, *Synthesis of Hybrid Organic-Inorganic Materials from Interpenetrating Polymer Network Chemistry,* Chem. Mater. **8** (1996) 727-733.
[38] T. Kokubo, *Bioactive glass ceramics: properties and applications*, Biomater. **12,** 1 (1991) 55–63.
[39] H, F. Hazenkamp, A. M. H. Van der Veen, W. Feiken, G. Blasse, *Hydrated rare-earth-metal ion-exchanged zeolite A: characterization by luminescence spectroscopy. Part 1. - The Gd^{3+} ion,* J. Chem. Soc. - Faraday Trans. **88,** 1 (1992) 133-140.
[40] D. K. Rice, L. G. Deshaser, *Spectral Broadening of Europium Ions in Glass*. Phys. Rev. B **186** (1969) 387-392.
[41] R. Reisfeld, *Fluorescence and Nonradiative Relaxations of Rare Earths in Amorphous Media and on High Surface Area Supports: A Review,* J. Eletrochem. Soc. **131** (1984) 1360-1364.
[42] G. Blasse, *Interaction between optical centers and their surroundings: an inorganic chemist's approach,* Adv. Inorg. Chem. **35** (1990) 319-402.
[43] F. S. Richardson, *Terbium(III) and europium(III) ions as luminescent probes and stains for biomolecular*

systems, Chem. Rev. **82** (1982) 541-552.
[44] R. Reisfeld, *Spectra and Energy Transfer of Rare Earths in Inorganic Glasses*, Structure Bonding **13** (1973) 53-98.
[45] A. I. Villacampa, J. M. G. Ruiz, *Synthesis of a new hydroxyapatite-silica composite material,* J. Crystal Growth **11** (2000) 111-115.
(Rec. 23/03/2010, Rev. 28/07/2010, Ac. 30/07/2010)